nature neuroscience

Subiculum neurons map the current axis of travel

Jacob M Olson, Kanyanat Tongprasearth & Douglas A Nitz

Flexible navigation demands knowledge of boundaries, routes and their relationships. Within a multi-path environment, a subpopulation of subiculum neurons robustly encoded the axis of travel. The firing of axis-tuned neurons peaked bimodally, at head orientations 180° apart. Environmental manipulations showed these neurons to be anchored to environmental boundaries but to lack axis tuning in an open arena. Axis-tuned neurons thus provide a powerful mechanism for mapping relationships between routes and the larger environmental context.

Hippocampal CA1 neurons are known for the location specificity of their action potential firing during free foraging within an arena[1]. Such location-specific firing is modulated by constraints governing running behavior and available trajectories[2–5]. In this way, CA1 can and does encode multiple navigationally relevant spatial relationships.

As an efferent target of CA1, the dorsal subiculum may be primed to encode more complex spatial relationships[6,7]. Subiculum neurons sometimes exhibit place-specific firing akin to that of CA1 (refs. 8,9), yet reported differences include increased generalization of place fields across environments, scaling of firing fields to match arena size, and increased numbers and sizes of fields[9–11]. Some subiculum neurons, termed boundary vector cells (BVCs), exhibit spatial tuning reflecting proximity and orientation to arena borders[12,13].

Multiple-pathway environments greatly increase the prevalence of task-relevant spatial relationships, but whether subiculum encodes such spatial features is unknown. We therefore obtained single-neuron recordings in rats performing a navigational task (**Fig. 1a** and **Supplementary Figs. 1** and **2**) wherein the layout of six interconnected routes ensured that each track section had a characteristic direction and axis of travel (**Fig. 1b**).

Immediately apparent from firing rate maps and directional tuning plots is a distinctive neuron subpopulation firing strongly whenever the animal ran in either of two opposing directions (**Fig. 1c**). Such firing was largely independent of room location. Put another way, such neurons fire when the animal travels in either direction along a single axis.

Since neurons with axis-tuned activity were not reported in work using open-field foraging tasks[8,13,14], we considered the possibility that axis-specific firing emerges during route running. Therefore, we also examined spiking activity during free foraging in an arena centered just atop the track environment with clear view of the same distal landmarks (**Fig. 1a**). Neurons with axis tuning on the track exhibited little evidence of axis-tuned firing in the arena (**Fig. 1c**). As previously observed[8,9,13,14], some subiculum cells exhibited spatially specific firing (**Supplementary Figs. 3** and **4**) akin to that of place cells in CA1 (~29%) and BVCs in subiculum (~21%).

To assess the prevalence of subiculum axis-tuned neurons, quantification of their characteristics is required. Such neurons should exhibit bimodal directional tuning peaks separated by 180°, and firing should be independent of environmental location (**Fig. 2a**). Therefore, we fitted von Mises mixture models of multiple orders to each neuron's firing data from half the recorded track traversals (**Supplementary Fig. 5** and Online Methods). Comparison of fits across multiple model orders allowed objective estimation of the prominent modes in the neural data. Cross-validation was applied to the remaining half of the data. The lowest-order model with a strong fit (>50% less error than a 0th-order circular model) and substantial improvement over the preceding model order (a further 20% error reduction) was chosen as the 'best' model. A higher proportion of subiculum neurons were categorized as bimodal (that is, second-order) than any other model order (**Supplementary Fig. 6**) across a wide range of model improvement criteria (10–22.5%). This bimodality bias existed in track-running but not arena free-foraging data. For neurons fit by a second-order model, thresholding for twice the firing at model maxima relative to minima removed weakly tuned neurons.

We also assessed the positional independence of bidirectional firing to quantify reliability in axis-tuned firing. Over track locations associated with either of the neuron's preferred tuning directions, we determined whether firing rate exceeded at least 50% of the mean rate for those same directions. Neurons were considered spatially independent if the majority of locations met this criterion.

The 47 neurons (of 542 tested) meeting these criteria were strongly tuned to a specific axis of travel on the track. Orientation separations between each neuron's two peaks overwhelmingly clustered near 180° (**Fig. 2b**). Tuning specificity was high, having a mean circular variance of 0.27 radians (± 0.08, s.d.). Firing rates at model-identified tuning peaks were, on average, 4.65 times those at tuning minima (± 2.23, s.d., outlier value of 90.4 removed; **Fig. 2c**). Thus, the actual strength in bimodal tuning was well above the applied criterion of a two-fold difference in firing. Mean spatial independence of axis-tuned firing was also well above criterion (73.9% ± 12.5, s.d.). Across this subpopulation, the preferred tuning directions of firing were evenly distributed (Hodges-Ajne uniformity test, $N = 94$, $P = 0.9182$; **Fig. 2d**).

Applying the same methodology and criteria, no neurons with strong axis-tuned firing were found in arena recordings (**Fig. 2e**,**f** and **Supplementary Figs. 6** and **7**). For a few neurons ($N = 8$), a first-order model identified a more moderate bias to a single direction both on the track and in the arena. For the 47 neurons identified as axis-tuned on the track, model maxima to minima ratios for the arena session were significantly lower ($N = 47$, $P = 1.79 \times 10^{-11}$, Wilcoxon rank sum test) and circular variance in peak tuning was significantly higher ($N = 94$, $P = 2.35 \times 10^{-18}$, Wilcoxon rank sum test). Spatial independence was unchanged ($N = 94$, $P = 0.07$, Wilcoxon rank sum test), consistent with axis-tuned firing on the track and the broad spatial tuning typical of subiculum arena data[8].

Department of Cognitive Science, University of California, San Diego, La Jolla, California, USA. Correspondence should be addressed to D.A.N. (dnitz@ucsd.edu).

Received 8 September; accepted 17 November; published online 19 December 2016; doi:10.1038/nn.4464

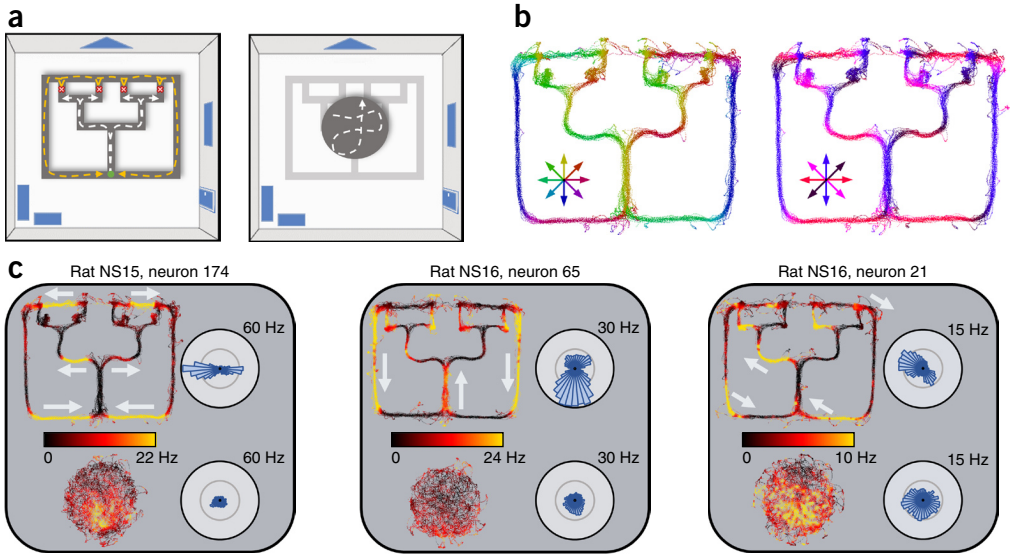

Figure 1 Axis-tuned firing of subiculum neurons. (**a**) Schematic of route-running and open-field foraging tasks. Left: animals made multiple runs along each of four partially overlapping routes (dashed white lines) on the 160 cm × 125 cm track apparatus, leading from a start site (green circle) to any of four goal sites (red circles). From each goal site, the animal returned to the start via either of two return paths (dashed yellow lines). Right: recordings were also obtained as animals foraged in a circular, 60-cm-diameter arena. Animals had clear view of the surrounding environment at all times. (**b**) Left: color-mapped mean directions of travel superimposed on representative tracking data. Right: color-mapped mean axes of travel (same recording). (**c**) Three example axis-tuned subiculum neurons. Each panel depicts firing rate color-mapped as a function of track position. White arrows mark directions and positions with highest firing. Each panel also depicts firing rate maps for the arena foraging session. Polar plots depict mean firing rate against head orientation. NS14, NS15 and NS16 designate the individual rats.

The preceding results indicate that the context of track-running and/or the constraints on available trajectories are critical in generating axis-tuned firing of subiculum neurons. As the track allowed clear view of distal visual cues along recording room walls, axis-tuned neurons could, in principle, anchor to either the recording room or the track structure. To determine which frame of reference served to anchor axis-tuned firing, a partially overlapping subset of neurons ($N = 170$) was also recorded following 90° track rotations (**Fig. 3a**). In all cases ($N = 26$), axis tuning was found to be anchored to the spatial frame of reference given by the recording room. Highly similar directional tuning plots were observed for the standard and rotated conditions in plots aligned to the room frame of reference (**Fig. 3b**). In this case, correlations between tuning curves for the two track configurations were high (mean 0.76 ± 0.16, s.d.). When the rotated track session's tuning curve was rotated to maintain the relationship to the track, mean correlations were far weaker (mean -0.41 ± 0.22, s.d.; $N = 26$, $P = 6.55 \times 10^{-10}$, Wilcoxon rank sum test; **Fig. 3c**).

Taken together, the present analyses of directional and spatial tuning properties of subiculum neurons reveal a previously unknown form of orientation encoding, the animal's axis of travel. Axis-tuned firing of subiculum neurons is recognized and quantified from directional tuning plots characterized by two distinct peaks in firing rate, separated by approximately 180°. Such axis-tuned firing: (i) can exhibit near complete independence from environmental location; (ii) is expressed primarily in the context of route-running along tracks as opposed to unconstrained movement in an open arena; and (iii) carries the environmental boundaries (allocentric space) as its spatial frame of reference. In addition, axis tuning persisted in darkness (**Supplementary Fig. 8**) suggesting that it is not strictly dependent on visual information and can be updated idiothetically. Subiculum axis-tuned neurons are clearly distinguishable from head direction neurons[15], whose activity maps only a single orientation and whose tuning is present during foraging in open arenas. Axis tuning is also distinguishable from boundary vector tuning because only a minority (7, or 14.9%) of the 47 axis-tuned neurons exhibited firing in the arena consistent with boundary vector encoding (**Supplementary Fig. 4**).

The context dependency of axis-tuned subiculum activity parallels that of several other forms of spatial representation. For hippocampal neurons, route running induces directional dependence in place-specific firing[2,3] and the emergence of trajectory-specific place fields[4,5]. The presence of high walls defining a 'switchback' path yields resetting of medial entorhinal cortex grid cell alignment across repeating route subspaces[16]. Finally, the action correlates of most posterior parietal cortex neurons in free foraging are replaced by route-position-dependent firing on tracks[17,18]. Thus, route running induces qualitative changes in spatial mapping in several brain structures and such changes yield conjunctive information concerning relationships between paths and the space of the larger environment. The neural mechanism gating the influence of movement directions in track-based versus arena environments remains a mystery.

The expression of axis-tuned subiculum activity in an environment having multiple interconnected paths is perhaps an initial clue to its functional significance. Axis-tuned activity encodes the track segment orientations relative to environmental boundaries. In humans, such route–boundary relationships can powerfully affect memory for the spatial layout of environmental landmarks[19]. In this sense, encoding of axis of travel could be particularly relevant in real-world environments where boundaries can be difficult to define. For example, a commonly used orientation tool in human navigation is to align oneself to a city's street grid based on a prominent, well-known, linear landmark such as a coastline, river or well-recognized street. In this respect, layering representation of movement axes atop the cognitive map provided by place and grid cells enhances its behavioral relevancy and therefore yields a more functionally complete mapping of space.

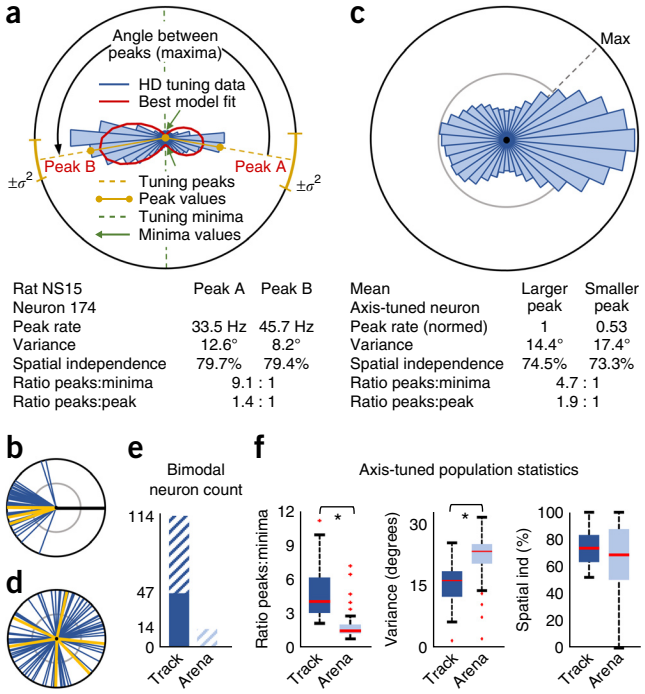

Rat NS15 Neuron 174	Peak A	Peak B
Peak rate	33.5 Hz	45.7 Hz
Variance	12.6°	8.2°
Spatial independence	79.7%	79.4%
Ratio peaks:minima	9.1 : 1	
Ratio peaks:peak	1.4 : 1	

Mean	Larger peak	Smaller peak
Axis-tuned neuron		
Peak rate (normed)	1	0.53
Variance	14.4°	17.4°
Spatial independence	74.5%	73.3%
Ratio peaks:minima	4.7 : 1	
Ratio peaks:peak	1.9 : 1	

Figure 2 Quantification of axis-tuned firing. (**a**) The same directional tuning plot as for the neuron in **Figure 1c** (left) is depicted again to describe axis-tuning metrics. A mixture model using two von Mises distributions (red ellipses) provided a good fit to the neuron's directional tuning plot. The model yields two tuning maxima at 100° and 260° from room north (dashed yellow lines; circular variances shown as yellow lines at the margin). Robustness and bias in tuning are given by maximum:minimum and maximum:maximum ratios, respectively. (**b**) For all 47 axis-tuned neurons, the directional tuning plots were aligned to the larger model peak of each neuron (black line). Blue lines depict the relative orientations of these neurons' opposite, smaller tuning peaks. Gold lines depict the second-peak orientations for **Figure 1c** neurons. (**c**) Mean of the maximum-normalized (normed) directional tuning plots for the 47 strongly axis-tuned neurons (plots aligned by the highest firing rate bin). (**d**) Orientations of all primary and secondary peaks relative to the space of the surrounding environment (**Fig. 1c** neurons in gold). (**e**) Cross-hatched bars depict the number of subiculum neurons (of 542) for which the second-order von Mises mixture model produced the best fits. Dark blue and light blue bars depict the number of neurons that also met criteria for ratio of directional tuning maxima versus minima and spatial independence ($N = 0$ neurons for the arena session). (**f**) Box plots of axis-tuned neuron population statistics (red bar, median; box limits mark first and third quartiles; whiskers extend to range of non-outlier data points). Peak-to-minimum ratios for axis-tuned neurons were significantly higher (left) for the track versus the arena recording epochs, whereas circular variance was lower (middle). Spatial independence (ind) of directional tuning was statistically similar (right). $^*P < 10^{-10}$.

METHODS

Methods, including statements of data availability and any associated accession codes and references, are available in the online version of the paper.

Note: Any Supplementary Information and Source Data files are available in the online version of the paper.

ACKNOWLEDGMENTS

The authors wish to thank the following people for technical assistance, discussion of the data, and editing of the original manuscript: E. Tao, J. Li, E. Mukamel, L. Quinn, L. Rangel, A. Chiba, A. Alexander, L. Shelley, D. Tingley, B. Voytek, R. Gao and J. Niebaum. This work was supported by the National Science Foundation (IOS-1149718) and the Kavli Institute for Brain and Mind (#2015-055).

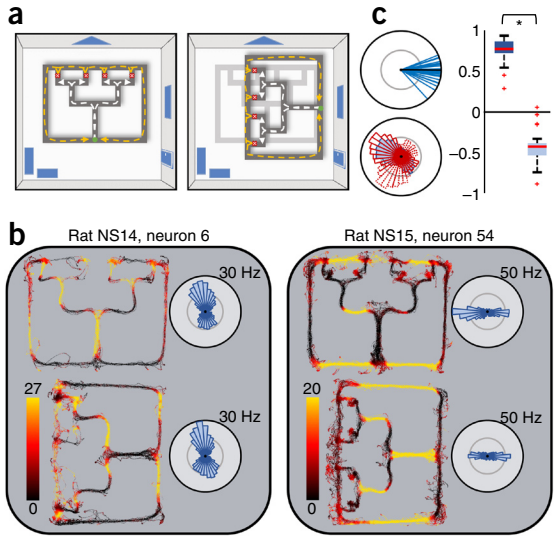

Figure 3 Spatial frame of reference for axis tuning. (**a**) The original (left panel) and rotated (right panel) track placements. (**b**) Color-mapped firing rates for axis-tuned neurons in the normal and rotated track configurations alongside the associated directional tuning plots. The neuron in the right panel is repeated from **Figure 1c** (upper left panel). Because tuning orientations persist, track positions yielding maximal firing differ substantially for the normal and rotated track orientations. (**c**) Comparison of orientation tuning across track orientations. Top left: alignments of tuning peaks during the rotated track session (blue lines, $N = 26$) relative to those for the same neurons during the normal track orientation session (the latter are all aligned to 90°). Bottom left: correlations between all directional firing rate values for the normal (blue) versus rotated (red) track conditions were compared to correlations between the same following 90° rotation of the values for the rotated track data (dotted red). Right: mean ($N = 26$) correlations between directional firing rate values for the normal and rotated track conditions (dark blue) and for the normal and rotated track conditions after 90° rotation of the rotated track data (matching track rotation in light blue; red bar, median; box limits mark first and third quartiles; whiskers extend to range of non-outlier data points). $^*P = 6.55 \times 10^{-10}$.

AUTHOR CONTRIBUTIONS

All authors contributed significantly to the design of experiments and analyses, data collection, and manuscript organization and writing.

COMPETING FINANCIAL INTERESTS

The authors declare no competing financial interests.

1. O'Keefe, J. & Dostrovsky *J. Brain Res.* **34**, 171–175 (1971).
2. McNaughton, B.L., Barnes, C.A. & O'Keefe, J. *Exp. Brain Res.* **52**, 41–49 (1983).
3. Markus, E.J. *et al. J. Neurosci.* **15**, 7079–7094 (1995).
4. Wood, E.R., Dudchenko, P.A., Robitsek, R.J. & Eichenbaum, H. *Neuron* **27**, 623–633 (2000).
5. Frank, L.M., Brown, E.N. & Wilson, M. *Neuron* **27**, 169–178 (2000).
6. O'Mara, S. *J. Anat.* **207**, 271–282 (2005).
7. Witter, M.P. *Behav. Brain Res.* **174**, 251–264 (2006).
8. Sharp, P.E. & Green, C. *J. Neurosci.* **14**, 2339–2356 (1994).
9. Kim, S.M., Ganguli, S. & Frank, L.M. *J. Neurosci.* **32**, 11539–11558 (2012).
10. Sharp, P.E. *Behav. Brain Res.* **85**, 71–92 (1997).
11. Sharp, P.E. *Behav. Neurosci.* **113**, 643–662 (1999).
12. Barry, C. *et al. Rev. Neurosci.* **17**, 71–97 (2006).
13. Stewart, S., Jeewajee, A., Wills, T.J., Burgess, N. & Lever, C. *Phil. Trans. R. Soc. Lond. B* **369**, 20120514 (2013).
14. Brotons-Mas, J.R., Montejo, N., O'Mara, S.M. & Sanchez-Vives, M.V. *Eur. J. Neurosci.* **32**, 648–658 (2010).
15. Taube, J.S., Muller, R.U. & Ranck, J.B. Jr. *J. Neurosci.* **10**, 420–435 (1990).
16. Derdikman, D. *et al. Nat. Neurosci.* **12**, 1325–1332 (2009).
17. Nitz, D.A. *Neuron* **49**, 747–756 (2006).
18. Whitlock, J.R., Pfuhl, G., Dagslott, N., Moser, M.-B. & Moser, E.I. *Neuron* **73**, 789–802 (2012).
19. McNamara, T.P., Rump, B. & Werner, S. *Psychon. Bull. Rev.* **10**, 589–595 (2003).

ONLINE METHODS

Subjects. All subjects were adult male Sprague-Dawley rats ($N = 3$). From these rats, a total of 542 subiculum neurons were recorded (81, 321 and 140 from each; see **Supplementary Fig. 1**). Rats were housed individually and kept on a 12-h light/dark cycle. Prior to experimentation, animals were habituated to the colony room and handled for 1–2 weeks. During training and experimentation, rats were food restricted and weights were maintained at 85–95% of free-fed weight with water available continuously. Rats were required to reach a minimum weight of 350 g (5–10 months of age) before surgery and subsequent experimentation. All experimental protocols adhered to AALAC guidelines and were approved by the IACUC and the UCSD Animal Care Program.

Statistical tests. The Hodges-Ajne Uniformity test is employed to consider potential bias in the distribution of directional tuning among the full population of neurons (**Fig. 2d**). The Wilcoxon rank sum test is employed to compare metrics for directional tuning of neural activity in the track-running versus arena foraging sessions (**Fig. 2f**); this test carries no assumption of normality in distribution of the data.

No statistical methods were used to predetermine sample sizes, but our sample sizes are similar to those reported in previous publications[17].

Data collection was not randomized, nor was analysis performed blind to the conditions of the experiment.

We here report exclusion of one value in calculating the mean for maxima to minima ratios across cells. Although no prior criterion was defined, the value is fully 19 times the mean and so clearly an outlier. Notably, this outlier was in the direction favoring a finding of significance in the statistical test applied and so its exclusion reflects a more conservative approach.

A **Supplementary Methods Checklist** is available.

Apparatus. Behavioral tasks were conducted using both a circular wall-less arena and a triple 'T' track maze. The track (**Fig. 1a**, left panel; 8-cm-wide pathways, overall 1.6 m × 1.25 m in length and width, painted black) stood 20 cm high in the middle of a large recording room and was visually open to prominent distal cues. The track edges were only 2 cm in height, allowing an unobstructed view of the environment. The arena (**Fig. 1a**, right panel, 60 cm in diameter) was placed 20 cm above the center of the track. The arena was also visually open to the same prominent distal cues as well as the track below. For the first recording of rat NS14 ($N = 17$ neurons), a high-walled pot (30 cm in diameter, 22 cm walls) was used in place of the arena.

Behavior. Rats were habituated to the maze during two 30-min periods of free exploration. Animals were then trained to run ballistically from the midpoint of one of the long edges of the maze into the center of the apparatus and continue until reaching the long edge opposite the start point (**Fig. 1a**, white dashed lines). This consisted of straight sections interleaved with three left or right turns for a complete path run. The total path lengths were 140 cm, with turns at 51 cm, 87 cm and 118 cm. Reward (a half piece of Cheerios cereal) was made available at the four reward sites. Over 1–2 weeks, animals were trained by approximation to make route traversals between food reward sites. Over at least 2 additional weeks, animals were trained by simple trial and error to a criterion of 80% for ballistic (uninterrupted) path traversal. Once animals met criterion, they were trained two or three times on the track in the normal orientation, immediately followed by training on the track in the 90° rotated orientation. This established familiarity with the rotated track, but the rats were not extensively trained in this orientation. Animals were surgically implanted only after this level of task performance had been achieved.

Multiple reward tasks were used across the set of animals. In an all-but-repeats task, used for animal NS14, the animal was rewarded at any of the four locations except when the animal repeated the same location as the previous run. In a visit-all task used for NS15 and NS16, the animal was rewarded at all locations, but needed to visit all locations before rewards were reset at all paths.

In the arena, two different behavioral epochs were used, each for approximately half of the time in the arena (~5 min each epoch). For the first half of the time, the animal was cued to make trajectories across the full arena for a 1/4 Cheerio's cereal reward at the track edge. The trajectory orientation was varied in order to obtain adequate sampling of the full arena surface. This pattern produced running activity similar to that on the track apparatus. The second half of each arena session was free foraging for small pieces of Cheerios reward dispersed randomly in the arena. Data were analyzed together in all portions of the paper to maximize sampling.

Surgery. Rats were surgically implanted with tetrode arrays (twisted sets of four 12.5-μm nichrome wires) inserted into custom-built microdrives (four to eight tetrodes per microdrive). Rats were implanted bilaterally with two or three microdrives into dorsal subiculum. Rats were anesthetized with isoflurane and positioned in a stereotaxic device (Kopf Instruments). Following craniotomy and resection of dura mater, microdrives were implanted relative to bregma (A/P −5.6 to −6.6 mm, M/L ±1.6 to ±2.7 mm, D/V −1.5 to −2.2 mm).

Recordings. After recovery from surgery, animals were retrained for at least 1 week before beginning recordings to ensure adequate behavior and running ability with the new weight of the implant. Because of this procedure, all recordings were from animals that were well trained on the task. Electrodes were moved ventrally in 40-μm increments between recordings to maximize the number of distinct units collected. Each microdrive had one or two electrical interface boards (EIB-16, Neuralynx) connected to a single amplifying headstage (20×, Triangle Biosystems). A tether led to a set of preamplifiers (50×) and a high pass filter (>150 Hz). Signals then fed into the acquisition computer running Plexon SortClient software and were filtered at 0.45–9 kHz, further amplified 1–15× (to reach a total of 1,000–15,000×), and digitized at 40 kHz. Single units were isolated in Plexon OfflineSorter software. Waveform parameters used were peak height, peak valley, energy, full width at half maximum, and principal components. Waveform clusters appearing to overlap with the amplitude threshold set for collection were discarded to avoid collection of neurons with partial spiking data. Waveform amplitudes were monitored to ensure systematic fluctuation did not produce confounds in isolating single units.

After completing unit isolation, a modified isolation distance value was calculated for each unit to assess cluster quality. Introduced by Harris *et al.*[20], isolation distance measures the separation of clusters by finding the Mahalanobis distance, reported in units of cluster variance, of the *n*th closest noncluster spike, where *n* is the number of spikes in the cluster. Put another way, isolation is the size from the center of the cluster to the circle that includes double the number of spikes as actually classified in the cluster. Accordingly, this measure is undefined when the number of the spikes in the cluster exceeds the number of spikes out of the cluster, and starts to lose intuitive meaning as a measure of distance to the nearest cluster as this limit is approached. Because of the propensity of high firing subiculum neurons, we have adapted this measure to be the minimum of the isolation distance as defined by Harris *et al.* and the distance to the noncluster spike 20% into the noncluster spike distance distribution. This modification to isolation distance serves to define the value for all neurons and to reduce the isolation distance for clusters with many spikes. While only reducing our neurons' scores, we believe this conservative adjustment more accurately represents cluster quality in these situations.

Animals' position was tracked using a camera set 2.6 m above the recording room floor. Plexon CinePlex Studio software was used to detect red and blue LED lights placed on the animal's surgical implant, centered on the animal's head and separated by approximately 5 cm. Position location of the lights was captured at 60 Hz. The animal's position and orientation was determined by averaging the location of the two lights and calculating the orientation of the vector between the lights. Using the fact that the track apparatus was squared to the room, we averaged the orientation of all time periods with >3 cm/s running and positions on the middle half of the return arms of the track. This angle was defined as 0°, or 'room north', for the recording and was used to align the animal's heading to the room. Recordings lasted approximately 45 min for arena and track recordings and 1 h 15 min for recording sessions with track rotation data. The animal would run in the arena for 3–10 min and then on the track for approximately 80 rewarded runs (**Fig. 1a**). For track rotation recordings, the animal had access to water for 5 min after completing the first session while the track was wiped down and rotated and then ran for another 80 rewarded runs (**Fig. 3a**). For dark recording, we began by running the animal on the typical arena and track sessions. Then the same protocol for a track rotation recording was carried out except the track was not rotated and only a red LED was used on the animal's implant. All other light sources in the room were turned off or covered. All other recording details were identical to other recordings.

We recorded a total of 542 subiculum neurons across three rats. For the first animal, all 81 neurons were recorded from the right hemisphere. For the second animal, 127 neurons were recorded from left subiculum and 194 from right subiculum. For the third animal, 42 and 98 neurons, respectively, were obtained from medial and lateral tetrode bundles in the right hemisphere. No neurons were excluded from analysis, even if activity was minimal.

Histology. Animals were perfused with 4% paraformaldehyde (vol/vol) under deep anesthesia. Brains were removed and sliced into 50-µm sections and Nissl-stained to reveal the final depth of electrode wires in subiculum. Microdrive depth monitored across recordings and final electrode depth as observed in histology were compatible in all cases.

Directional tuning vectors. Head direction tuning vectors were calculated using the same sample of running data as the positional firing rate maps (i.e., using the same velocity thresholds). Head orientations were binned into 36 10° bins. The total number of spikes per bin was divided by the total time in each bin to calculate the mean directional firing rate.

Orientation maps. Orientation maps (**Fig. 1b**) were created by calculating the mean circular direction[21] of all samples at each spatial location.

Positional firing rate maps. To characterize the firing activity of the subiculum neurons, we calculated individual neurons' positional firing rates by dividing the total number of spikes of each neuron at each location by the total occupancy time at each location. To include only data where the animal was running, we excluded all samples with less than 3 cm/s velocity or greater than 20 radians/s angular velocity. The latter threshold was used to exclude cases of rapid head turning in the absence of locomotion. Positional firing maps were smoothed using a 2D convolution with a Gaussian filter with s.d. of 2 cm that also accounts for bins with no occupancy[22]. Raw, unsmoothed data were downsampled to 2 cm × 2 cm bins for analysis of spatial independence of directional firing. For **Supplementary Figures 3**, **4** and **7**, data were downsampled to 2 cm × 2 cm bins and smoothed using a 2D convolution with a Gaussian filter with s.d. of 4 cm and the same occupancy adjustment as above.

Burst index for spiking activity. To assess burstiness in subiculum spiking activity, we applied the method outlined and used by Kim *et al.* (2012)[9]. We did this for two reasons. First, the method developed by Kim *et al.* is not confounded by firing rate differences, a key factor considering the diverse firing rates of subiculum neurons. Second, using the same method allowed direct comparisons of our results to previous findings. The burst index is computed by integrating the spike autocorrelogram from 1–6 ms and dividing the result by the integrated power from 1-20 ms. The measure allowed us to demonstrate that the basic firing properties of subiculum neurons recorded in our work are in line with those observed previously[9].

Arena spatial measures. Arena spatial firing was described using three classic spatial measures: spatial information[23], spatial information per spike[23] and spatial coherence[24]. All analyses were implemented as described in the respective sources on arena data downsampled to 2 cm × 2 cm bins. Only those neurons with at least 250 spikes in the arena ($N = 354$ of 542) were analyzed. Briefly, spatial information is the number of bits of information per second the neuron communicates while the animal is on the arena. Spatial information per spike is this same value but now as a rate of bits per spike of the neuron. This reframing is useful for neural populations with low variability in firing rates, but greatly skews values against high-firing neurons in more variable populations. For this reason, we primarily utilize spatial information in this paper. We do include information per spike for the sake of comparison to other work. Finally, spatial coherence is the Pearson correlation of all locations on the arena to the mean of their surrounding locations. Coherence is a measure of smoothness of firing activity across space and is high for spatially reliable neurons provided binning is adequately small.

Spatial correlates (BVC and place) model comparison. Both place cell and boundary vector cell (BVC) spatial representations have been previously described in dorsal subiculum[8]. To better describe the prevalence and form of strong spatial tuning in the open arena, we devised a brute-force template-matching procedure that compares the 2D spatial firing rate map of each neuron to a set of all possible ideal place and BVC firing maps.

The 2D firing rate map templates for BVCs were formed by following the BVC-defining model equations provided in Hartley *et al.*[25]. As stated in Hartley *et al.*[25], equation 1, the receptive field $g(r,\theta)$ of a BVC tuned to a boundary distance d and a bearing ϕ from the rat is

$$g(r,\theta) \propto \frac{1}{\sqrt{2\pi\sigma^2_{\mathrm{rad}}(d)}} e^{\frac{-(r-d)^2}{2\sigma^2_{\mathrm{rad}}(d)}} \times \frac{1}{\sqrt{2\pi\sigma^2_{\mathrm{ang}}}} e^{\frac{-(\theta-\phi)^2}{2\sigma^2_{\mathrm{ang}}}}$$

where r is the distance and θ is the bearing to that boundary. By using Hartley *et al.*'s[25] equation 2, the firing rate of a BVC at any Euclidian location $f(x,y)$ is calculated by summing the contribution of all boundaries:

$$f(x,y) = \sum_b g(r_b,\theta_b) \times \Delta\theta$$

where b is one instance from the set of all boundaries. We calculated the distance and orientation to the edge of the arena at 5° increments ($\Delta\theta = 5°$) for each location and used this as our set of boundary distances and orientations. We defined $\sigma^2_{\mathrm{ang}} = 0.2$ radians to mimic the settings of Hartley *et al.*[25], although it is worth noting any reasonably small value gives similar results. Hartley *et al.*[25] define σ^2_{rad} as

$$\sigma_{\mathrm{rad}} = \frac{d}{\beta+1}\sigma_0$$

so that σ^2_{rad} varies linearly with distance. We used $\beta = 10$ and σ_0 at 4 values, $\sigma_0 = [0.25, 0.5, 0.75, 1]$, to allow the model a variety of distance tolerances and remain as agnostic as possible about predicted parameter values. The final free parameter, d, is the BVC's preferred distance to the border. Allowing any reasonable parameter values as was done with σ_0, we chose d values from distance 0 (the edge of the arena) to the arena radius (30 cm) at 4-cm intervals, resulting in 9 distances. Finally, creating BVCs by combining all possible orientations (72, 5° increments), σ_0 values (4), and feasible distances (9), we created ~2,500 ideal BVC firing rate maps per neuron.

The 2D firing rate map templates for place cells was a similar procedure. A 2D Gaussian distribution was used to create templates with centers at each 2 cm × 2 cm bin location. As in the BVC models, we used 4 s.d. values for each location: σ = 5, 7, 9 and 11 cm. This resulted in ~2,800 ($\pi r^2 \times 4$, where r is in bins) place cell templates per neuron.

To assess the fit of a neuron to a place cell or BVC model, we ran a Pearson correlation on all bins with occupancy and their corresponding values in all BVC and place cell templates. We then selected the template with the highest r value for each of the BVC and place cell template sets and used this as our estimate of the quality of fit of each cell type to our data. We did this for all 354 neurons with at least 250 spikes on the arena. As nearly all neurons displayed significance as compared to a bootstrap method creating 1,000 shuffles of the same neuron's firing rates before correlating with the templates, we arbitrarily chose a higher Pearson $r = 0.4$ cutoff value to determine spatial model correlation. This value was chosen by visual inspection as a threshold where neurons with higher r values did often fit the templates reasonably well.

Fitting of von Mises mixture models. To fit direction tuning data, we used von Mises distributions, a periodic generalization of the Gaussian distribution. For a von Mises distribution evaluated at angle x, centered at mean angle μ and with concentration κ, the probability density function $f_{\mathrm{vm}}(x \mid \mu,\kappa)$ is

$$f_{\mathrm{vm}}(x \mid \mu,\kappa) = \frac{e^{\kappa\cos(x-\mu)}}{2\pi I_0(\kappa)}$$

where $I_0(\kappa)$ is the modified Bessel function of the first kind of order 0. The dispersion, $1/\kappa$, is analogous to variance. If $\kappa = 0$, the distribution is uniform, and as κ increases, the distribution approaches the normal distribution with mean μ and variance $1/\kappa$. Because our data potentially displayed multiple peaks, a mixture of von Mises distributions with multiple means and variances were fit and compared. The von Mises mixture model for orientation x is

$$f_{\mathrm{vmm}}(x \mid \mu,\kappa,\pi) = \sum_{j=1}^{M} \pi_j f_{\mathrm{vm}}(x \mid \mu_j,\kappa_j)$$

doi:10.1038/nn.4464

which is a weighted sum of multiple von Mises distributions of varying means and dispersions. We define π_j as the weight of the jth model in the mixture model of order M. Bold denotes a vector of all of the values for the corresponding von Mises models. The order of the von Mises mixture model is the number of combined von Mises distributions. The 0th-order model is equivalent to a uniform circular distribution whose values, like those of the normalized rate data, sum to 1. Order 1 to order 8 models employ one to eight von Mises distributions, respectively. Model orders up to 8 were included so that all reasonably feasible multimodal possibilities given the empirical width of tuning peaks were evaluated.

For each condition (arena, track standard and track rotated) and neuron, a directional tuning vector was calculated from a randomly selected half of the data as described in "Directional tuning vectors" above. Mean firing rates were converted to a proportional number of data samples in the mean direction for each bin. Then, separately for each order model from 1–8, we implemented the estimation-maximization algorithm[26] to find a model fit to the data. The estimation-maximization algorithm for a von Mises mixture model has already been applied and used in audio source research[27]. It can be described in four steps:

1) Initialize parameters for the each of the von Mises distributions in the model. We initialized the means by separating the means as far as possible on the circle, given the order of the model being used. So, for a fourth-order model, means were initially located 90° apart. Concentration values scaled linearly with the number of distributions. This was done to keep distribution overlap at initialization relatively similar across the model orders. Finally, the mixing parameter was always set to equal probabilities for all models. To account for the possibility that mean initialization orientations effected the outcome, we offset our equally spaced distributions at 10 equal offsets between the original model locations and ran the algorithm with each initialization. The model with the lowest log likelihood was the one used for further analysis.

2) Estimation step: evaluate the responsibility γ each von Mises distribution model has in the prediction of each of N data points

$$\gamma_{ij} = \frac{\pi_j \; f_{\mathrm{vm}}\left(x_i \mid \mu_j, \kappa_j\right)}{\sum_{m=1}^{M} \pi_m \; f_{\mathrm{vm}}\left(x_i \mid \mu_m, \kappa_m\right)}$$

where γ_{ij} is the responsibility of the jth von Mises distribution in the model for the ith data point, x_i.

3) Maximization step: re-estimate the parameters μ, κ and π using the current responsibilities γ. Specifically, this is done by solving the following equations for each of the means

$$\mu_j = \tan^{-1} \frac{\sum_{i=1}^{N} \gamma_{ij} \sin\left(x_i\right)}{\sum_{i=1}^{N} \gamma_{ij} \cos\left(x_i\right)}$$

the concentrations

$$A\left(\kappa_j\right) = \frac{I_1\left(\kappa_i\right)}{I_0\left(\kappa_i\right)} = \frac{\sum_{i=1}^{N} \gamma_{ij} \; \cos\left(x_i - \mu_j\right)}{\sum_{i=1}^{N} \gamma_{ij}}$$

and the mixture parameters

$$\pi_j = \frac{1}{N} \sum_{i=1}^{N} \gamma_{ij}$$

for each von Mises distribution in the model. Please note that κ_j is best solved by numerically inverting the defined function $A(\kappa_j)$.

4) Check for convergence of the log likelihood of the data given the model. We quit when the log likelihood improved by less than 0.01%. If convergence is not reached, update the parameter values using the newly calculated parameters and repeat steps 2 and 3.

Evaluation of von Mises mixture model fit. For each neuron, each model was cross-validated by calculating the sum-squared-error (SSE) between model values and actual direction tuning values for the remaining half of the data. The ratio of SSE of each order mixture model to SSE of the circular (0th-order) model for that same neuron was used to determine overall goodness of fit. Taking into account the trade-off between model fit and model complexity, we defined the 'best' model as the model yielding a 50% improvement in fit over the circular model and a 20% improvement over the next simplest model. Similar results were obtained using thresholds of 40–60% improvement over the circular model and 10–22.5% improvement over the next simplest model (**Supplementary Figs. 5** and **6**).

Spatial independence. The spatial independence criterion was used to identify neurons that were consistently active when the animal was facing a preferred orientation regardless of spatial location on the track. For all 2 cm × 2 cm spatial bin locations with at least 10 samples in a peak 10° bin orientation, the neuron was considered active if its mean rate at that position and orientation was at least 50% of its overall mean rate for that orientation. If more than 50% of the viable locations for both peaks of a neuron were active, the neuron was considered to meet this criterion.

Maxima and minima orientations and ratios. Peak orientations are the von Mises mixture model orientation parameters. Large and small peaks are determined by the mixture parameters of the model. Maxima and minima values for ratio calculations are determined by actual data values from the orientation bins containing the model maxima and minima. Peak-to-minimum ratios are the mean of the peak values divided by the mean of the minima values. Peak-to-peak ratios are simply the larger peak value divided by the smaller peak value.

Correlation across track positions. Pearson correlations for the track rotation experiment were calculated between the directional tuning vectors of the track data in the normal orientation and directional tuning data from the 90°-rotated track session for each individual neuron. Pearson correlations were also calculated between the normal track orientation data and the 90°-rotated track data shifted 90°. A Wilcoxon rank sum test was run between the two populations for the axis-tuned subpopulation.

Alignment of peaks. Peak alignments for the track rotation experiment were calculated using the angle difference between the larger peak on the non-rotated track and the closest peak on the rotated track.

Data and code availability. The data that support the findings of this study and code used for analysis are available from the corresponding author upon reasonable request.

20. Berens, P. *J. Stat. Softw.* **31**, 1–21 (2009).
21. Harris, K.D., Henze, D.A., Csicsvari, J., Hirase, H. & Buzsáki, G. *J. Neurophysiol.* **84**, 401–414 (2000).
22. Krause, B. Nanconv.m *MATLAB Central File Exchange* http://www.mathworks.com/matlabcentral/fileexchange/41961-nanconv (2013, retrieved 15 January 2016).
23. Skaggs, W.E., McNaughton, B.L., Gothard, K.M. & Markus, E.J. An information-theoretic approach to deciphering the hippocampal code. in *Advances in Neural Information Processing Systems* Vol. 5 (eds. Hanson, S.J., Cowan, J.D. & Giles, C.L.) 1030–1037 (1993).
24. Kubie, J.L., Muller, R.U. & Bostock, E. *J. Neurosci.* **10**, 1110–1123 (1990).
25. Hartley, T., Burgess, N., Lever, C., Cacucci, F. & O'Keefe, J. *Hippocampus* **10**, 369–379 (2000).
26. Dempster, A.P., Laird, N.M. & Rubin, D.B. *J. R. Stat. Soc. Series B Stat. Methodol.* **39**, 1–38 (1977).
27. Park, T. & Lee, T. Multichannel audio signal source separation based on an interchannel loudness vector sum. Preprint at https://arxiv.org/abs/1512.08075 (2015).